-Bi_2O_3 nanorods: synthesis, characterization and UV-photocatalytic activity

2017 Mater. Res. Express 4 035039

(http://iopscience.iop.org/2053-1591/4/3/035039)

Materials Research Express

PAPER

α-Bi_2O_3 nanorods: synthesis, characterization and UV-photocatalytic activity

Ahmed M Abu-Dief[1] **and W S Mohamed**[2]

[1] Faculty of Science, Chemistry Department, Sohag University, 82524 Sohag, Egypt
[2] Faculty of Science, Physics Department, Sohag University, 82524 Sohag, Egypt

E-mail: wael-saad@science.sohag.edu.eg

RECEIVED
21 January 2017

REVISED
26 February 2017

ACCEPTED FOR PUBLICATION
15 March 2017

PUBLISHED
29 March 2017

Keywords: α-Bi_2O_3, nanorods, TEM, FTIR, photocatalyst

Abstract

In this study, Monoclinic bismuth oxide nanorods (α-Bi_2O_3 NRs) were successfully synthesized by a simple one-step hydrothermal route using (water: ethanol) (1:1) as a mixed solvents at optimum conditions. The Bi_2O_3 nano-powder was characterized in detail by different techniques in terms of their structural, morphological, compositional, optical and photocatalytic properties. X-ray diffraction (XRD) analysis indicated that the as-synthesized Bi_2O_3 NRs exhibited high purity with monoclinic structure (α-Bi_2O_3) and good crystallinity. The Transmission electron microscope (TEM), Energy dispersive x-ray spectroscopy (EDXS) and Field Emission scanning electron microscope (FE-SEM) analysis clearly confirmed the high purity and the nanorod morphology of the as-synthesized Bi_2O_3 sample. The optical band gap of α-Bi_2O_3 NRs was estimated using the UV–Vis diffuse reflectance spectroscopy (UV–Vis DRS) analysis according to the Kubelka–Munk theory. The optical band gap of α-Bi_2O_3 NRs was found to be 3.55 eV for an indirect allowed transition and 3.63 eV for a direct allowed transition. The Fourier transfer infrared spectroscopy (FTIR) was employed to check the structure as well as to evaluate the phonon vibration modes corresponding to Bi_2O_3. Photocatalytic activity of α-Bi_2O_3 NRs was investigated using UV source lamp. The as-synthesized α-Bi_2O_3 NRs photocatalyst exhibited better performance for degradation and decolorization of Methylene blue (MB) under ultraviolet (UV) irradiation. MB was completely photodegraded after 210 min under UV irradiation using α-Bi_2O_3 NRs as photocatalyst.

1. Introduction

Recent advancements in the synthesis of low-dimensional nanostructure semiconductor oxides, with various morphologies, were merited due to the potential which comes along their unique physical and chemical properties [1–8]. For instance, the physical and chemical properties of bismuth based materials, such as Bi_2O_3, $Bi_2Ti_2O_7$,$BiVO_4$,$BiNaO_3$, $Bi_2Sn_2O_7$, Bi_2WO_6, BiOCl, $Bi_2O_2CO_3$, Bi_2MoO_6, has been in the focus of comprehensive research due to their possible utilization in many applications [2, 9–15]. Bismuth oxide (Bi_2O_3) is considered the parent compound of the interesting bismuth-based material families; it also has a unique structure and useful chemical and physical properties such as structural stability, large band gap, high refractive index, large ionic conductivity, nontoxic nature, catalytic activities, excellent photoconductivity and high photoluminescence [16].

Bi_2O_3 crystallizes in six main crystallographic polymorphisms; two stable phases: low temperature α-Bi_2O_3 (monoclinic structure) and high temperature δ-Bi_2O_3 (cubic, face center structure); and four high-temperature metastable phases: β-Bi_2O_3 (tetragonal structure), γ-Bi_2O_3 (cubic, body centered structure), ε-Bi_2O_3 (orthorhombic structure) and ω-Bi_2O_3 (triclinic structure) [12, 17]. The transitions between various Bi_2O_3 phases are governed by the ambient temperature and the synthesis methods.

The photocatalytic activity of Bi_2O_3 comes from its ability to oxidize organic pollution and produce highly reactive species, such as O^- and $OH^{\blacksquare}$ radicals. Moreover, at nano-scale, Bi_2O_3 exhibits peculiar properties that may be targeted during fabrication in order to enhance their utilization. Which enables Bi_2O_3, with different polymorphisms, to be found in many current and future applications, such as solar cells, gas sensors, optical coating, optoelectronics and photocatalytic degradation of organic dyes [12, 18, 19]. For example, shape, size, orientation and physical properties of nanoparticles heavily affect the photocatalytic activity of the investigated materials, which may be associated to its wide surface area and the presence of vacancies and uncoordinated atoms at edges and corners of crystal structure.

Bi_2O_3 nanostructure materials can be synthesized by numerous physical and chemical methods, i.e. pulsed laser deposition (PLD) [20], Epitaxial growth [21], thermal plasma [22], magnetron sputtering [23], vapor transport method [24], chemical precipitation [25], chemical vapor deposition [26], metal-organic chemical vapor deposition (MOCVD) [27], sonochemical [16] and hydrothermal [28]. For large scale manufacturing and Industrial purposes, chemical methods are mainly sough to synthesize Bi_2O_3 nanostructure materials. Among them is the hydrothermal method, which is superior in many aspects such as simplicity of implementation, efficiency and flexibility in addition, the hydrothermal method produces high product purity and homogeneity with unique properties including narrow particle size distributions, crystal symmetry and high dispersibility [29].

In this work, we report the synthesis of α-Bi_2O_3 NRs—which to the best of our knowledge the UV-photocatalytic activity of α-Bi_2O_3 structure has not been fully studied—by a simple one-step hydrothermal route. X-ray diffraction (XRD), energy dispersive x-ray spectroscopy (EDXS), Field Emission scanning electron microscope (FE-SEM), transmission electron microscope (TEM), UV–VIS–NIR spectrophotometer and Fourier transfer infrared spectroscopy (FTIR) were used to confirm and investigate the different physical properties of Bi_2O_3 NRs. The photocatalytic response of as-synthesized α-Bi_2O_3 NRs as promising photocatalyst was checked using the degradation of Methylene blue (MB) under ultraviolet irradiation.

2. Experimental methods

2.1. Materials

All reagents which used in the investigation were analytical grade and used without further purification. Bismuth (III) nitrate pentahydrate $Bi(NO_3)_3 \cdot 5H_2O$ (Sigma-Aldrich) was the Bismuth precursor, while NaOH (pellets, 98%, Alfa Aesar) was the precipitating agent and solvents (absolute ethanol and acetone) were used for washing the formed precipitate.

2.2. Synthesis of Bi_2O_3 nanorods

Bi_2O_3 Nano powder was prepared according the following procedures: $Bi(NO_3)_2 \cdot 5H_2O$ was dissolved in 30 ml (water:ethanol) (1:1) and stirred magnetically until dissolved completely. After that, the pH was adjusted to 12 by adding NaOH (2M) drop-by-drop. After 1 h under continuous stirring, a homogeneous solution containing hydroxide precipitate was obtained. Finally, the resulted reaction mixture (total volume 80 ml) were sealed in Teflon-lined stainless autoclaves, heated at 180 °C for 20 h, and then cooled to room temperature (RT) gradually. The obtained products were centrifuged, washed several times with bi-distilled water, acetone and absolute ethanol, and then dried at 80 °C for 5 h. Taken solid phase sample was ground in a mortar to powder it. Then, the obtained powder was used further for all of the measurements.

The following Scheme summarized the formation of Bi_2O_3 Nano powder:

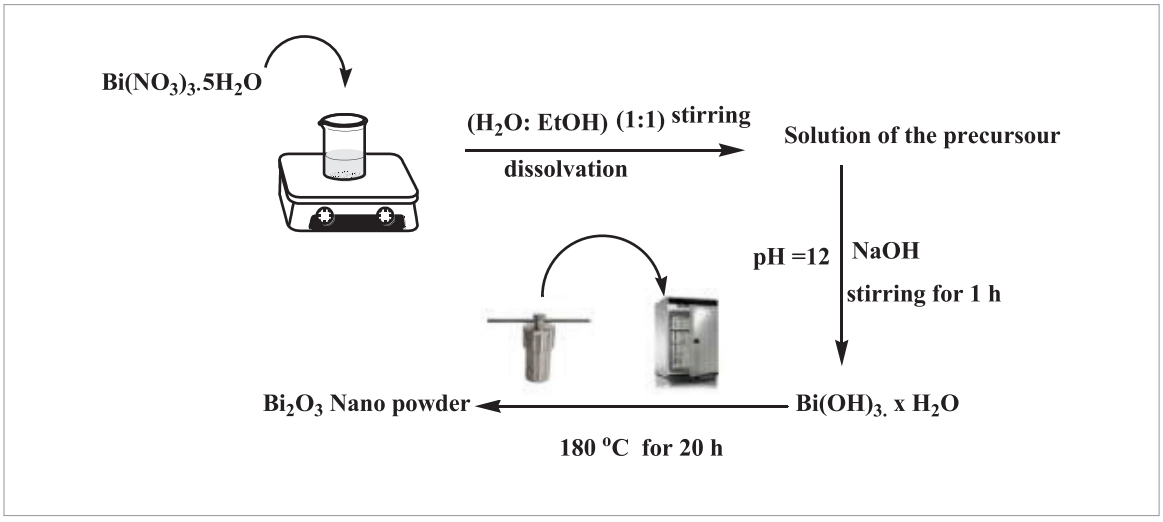

2.3. Characterization

Crystallographic structure of Bi_2O_3 nano-powder was investigated by x-ray powder diffraction (XRPD) using a PANalytical's X'Pert PRO MRD x-ray diffractometer with a high intensity CuKα radiation ($\lambda = 1.5418$ Å). The samples were gently ground in an agate mortar to reduce the required orientation. For typical powder patterns, all data were collected at 2θ from ~10° to 70° with a step of 0.05° and counting time of 2.5 s/step. The instrumental resolution was determined by using LaB6 standard reference material (SRM 660a) provided by National Institute of Standards and Technology (NIST), which is generally used for calibrating line position and line shape in

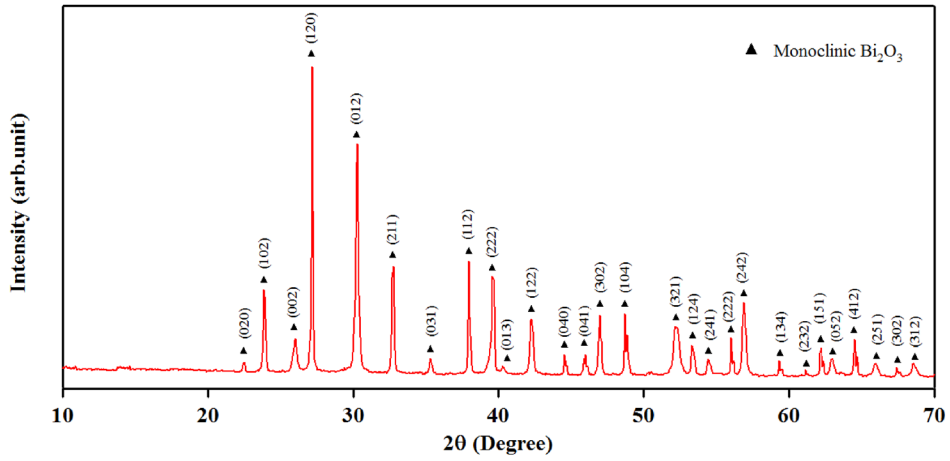

Figure 1. Typical XRD pattern of α-Bi_2O_3 nanorods. Note: the numbers above the peaks correspond to the miller indices (*hkl*) values of the monoclinic Bi_2O_3 structure.

powder diffractometers. The chemical composition of α-Bi_2O_3 NRs were investigated using scanning electron microscope (SEM), (Model: JEOL 6610VL) supplied with an x-max silicon drift detector for energy dispersive x-ray spectroscopy (EDXS) analysis, with an accelerating voltage of 20 kV. The nanorod morphology of the Bi_2O_3 samples was investigated using field emission-scanning electron microscope (FE-SEM, Model: Quanta 250 FEG) and transmission electron microscopy (TEM) (Model: a JEOL-JEM-2100F) operated at an accelerating voltage of 200 kV. The samples for TEM were dispersed in ethanol under sonification and sprayed on a carbon-coated copper grid and then allowed to air-dry, finally, Gatan SOLARUS 950 was used before observation. The optical energy gap of α-Bi_2O_3 NRs as well as the concentration of MB were investigated using a double-beam UV–VIS–NIR spectrophotometer (Model: JASCO, V-570) equipped with a diffuse reflectance (DR) accessory (Model: JASCO, ISN-470), in the wavelength range between 200 and 2500 nm at normal incidence. Moreover, infrared absorption spectra of α-Bi_2O_3 NRs were investigated using Fourier transform infrared spectroscopy(FT-IR) using the technique of KBr pellet, in the wavelength range of 400–4000 cm^{-1}.

2.4. Potocatalytic activity measurements

The Photocatalytic activity of the as-synthesized α-Bi_2O_3 NRs is evaluated by the following of photocatalytic degradation of Methylene blue (MB) dye under ultraviolet (UV) irradiation (40 W, 280 nm–100 nm UV-C Germicidal lamp with main emission wavelength 254 nm). In a typical experiment, 50 mg of the α-Bi_2O_3 NRs photocatalyst was dispersed in 100 ml MB aqueous solution at a concentration of 10 mgl^{-1} to produce a suspension for the degradation reaction. Before exposure to illumination, the obtained solution was magnetically stirred in dark for 70 min to acquired adsorption–desorption equilibrium between dye and catalyst. All experiments were carried out at RT under constant magnetic stirring and natural pH conditions. During the UV irradiation and at given time intervals (30 min) about 4 ml of suspension was sampled by syringe and subsequently centrifuged using an eppendorf centrifuge model (Hettich-EBA 20) for 5 min at a rate of 4000 rpm to remove photocatalyst powder from the MB solution.We were repeated the centrifuge process three times more to make sure that the solution free of catalyst particles and between every two runs, the suspension was transferred to a clean eppendorf centrifuge tube to remove photocatalyst powder from the MB solution.Finally, in order to follow the degradation of the MB, the absorption spectra and then the concentration of MB in the UV–Vis region were monitored by Jasco, V-570 UV–Vis–NIR Spectrophotometer, with ultra-pure water as the reference medium.

3. Results and discussion

3.1. XRD analysis

The phase crystallinity and purity of the as-synthesized Bi_2O_3 powder sample were investigated using XRD analysis. Figure 1 displays the powder XRD diffractograms of Bi_2O_3 sample, which shows strong and sharp diffraction peaks, inferring a high degree of crystallization of the Bi_2O_3 crystals. Moreover, no other secondary crystalline phases were detected by XRD, indicating the high purity of the as-synthesized product. All diffraction peaks in the XRD pattern of powder sample strongly indexed to monoclinic phase (α) of Bi_2O_3. Peak positions and their relative intensities are in good agreement with bulk monoclinic Bi_2O_3 crystal (JCPDS file No.41–1449). In figure 1 the peaks observed in the XRD patterns of α-Bi_2O_3 at 2θ values of 22.48°, 23.86°, 25.96°, 27.16°, 30.28°, 32.74°, 35.32°, 37.96°, 39.58°,40.3°, 42.22°, 44.56°, 46°, 46.96°,48.7°, 52.18°, 53.32°, 54.46°, 56.02°, 56.86°, 59.32°,

Table 1. The crystallographic parameters, dislocation density and micro-strain of as-synthesized α-Bi_2O_3 nanorods calculated from XRD analysis.

(2θ)	(hkl)	$(\beta_{2\theta})$ (radians)	(D_{avg}) (nm)	(δ_D) $(10^{15}$ Line · $m^{-2})$	(ε_m) (10^{-3})
27.16	120	0.18	47.4	0.45	0.76
30.28	012	0.23	35.8	0.78	0.97

61.12°,62.2°, 62.98°, 64.48°, 65.92°, 67.42° and 68.56° match perfectly with the (0 2 0), ($\bar{1}$ 0 2), (0 0 2), (1 2 0), (0 1 2), ($\bar{2}$ 1 1), (0 3 1), (1 1 2), ($\bar{2}$ 2 2), (0 1 3), (1 2 2), (0 4 0), (0 4 1), ($\bar{3}$ 0 2), ($\bar{1}$ 0 4), ($\bar{3}$ 2 1), ($\bar{1}$ 2 4), ($\bar{2}$ 4 1), (2 2 2), ($\bar{2}$ 4 2), ($\bar{1}$ 3 4), (2 3 2), (1 5 1), (0 5 2), ($\bar{4}$ 1 2), ($\bar{2}$ 5 1), (3 0 2) and (3 1 2) planes reported in JCPDS file No.41-1449, which indicates the sample phase is pure monoclinic Bi_2O_3, belonging to space group $P2_1/c$, with lattice parameters of $a = 5.8499$ A°, $b = 8.1698$ A°, $c = 7.5123$ A°. The average crystallite size (D_{avg}) (i.e. coherently diffracting domains) of the α-Bi_2O_3 NRs is calculated using the well-known Debye–Scherer formula [30, 31]:

$$D_{avg} = \frac{C\lambda}{\beta_{2\theta}\cos\theta} \tag{1}$$

where C is a constant taken to be 0.94, λ is the wavelength of x-radiation source (i.e. $\lambda = 1.5418$ Å), $\beta_{2\theta}$ is the full width at half maximum (FWHM) in radians along (1 2 0) and (0 1 2) planes and θ is the diffracted Bragg angle. We have estimated the average crystallite size of α-Bi_2O_3 NRs via XRD line broadening analysis using Origin 8.1 Software and PsdVoigt1 function in the fitting procedure as illustrated in table 1.

The dislocation density of the α-Bi_2O_3 NRs (δ_D), which represents the mount of crystallographic defect or irregularity within a crystal structure is determined according to the following expression [32, 33]:

$$\delta_D = \frac{1}{D_{avg}^2} \tag{2}$$

The Micro-strain (ε_m) is one of the most important parameters used to characterize powder samples, which describes the change in the microstructure, size and shape of the particles and is given by [34]:

$$\varepsilon_m = \frac{\beta_{2\theta}\cos\theta}{4} \tag{3}$$

The calculated structural parameters are presented in table 1. The small values of δ_D and ε_m obtained in the present study confirm the good crystallinity of the α-Bi_2O_3 NRs synthesized by the hydrothermal method.

3.2. EDXS, FE-SEM and TEM analysis

To investigate the elemental and compositional properties of the sample, the chemical composition of Bi_2O_3 sample was analyzed using energy dispersive x-ray spectroscopy (EDXS). The EDXS spectra of Bi_2O_3 sample and their related data (i.e. at two different positions 1 and 2) are shown in figure 2. In the EDXS spectra, we observe the absence but Bi, O and Au peaks, which was further indicated the high purity of the as-synthesized α-Bi_2O_3 NRs. The manifestation of Au peaks attributed to existence of the gold catalyst. The quantitative EDXS analysis indicates that the atomic ratios of Bi:O are 10.28:40.20 and 7.76:35.84 corresponding to positions 1 and 2 respectively, close to 1:4,which can approximately confirm the stoichiometric content of the product. Figure 3 shows the typical FE-SEM image of α-Bi_2O_3 NRs which indicates the rod-shaped morphology of the as-synthesis α-Bi_2O_3 nano-powder. Where, the nanorodes are grown in high density and have a random orientation. TEM investigation confirmed the nanorod morphology of the as-synthesized Bi_2O_3 sample.Typical TEM micrographs of α-Bi_2O_3 NRs with different magnifications were shown in figures 4(a)–(c), where nanorod like structure is clearly evident with smooth and clean surfaces. Figure 4(d) shows corresponding diameter distribution histogram of α-Bi_2O_3 NRs estimated by Imag J software and Excel calculation [35, 36]. The diameter of α-Bi_2O_3 NRs are in the range between 15 and 42 nm with an average diameter of 29 nm and length up to several micrometers, which are approximately consistent with those determinate via XRD line broadening analysis (see table 1).

3.3. FTIR analysis

FT-IR spectroscopy was employed to investigate the chemical bonding and quality of as-synthesized α-Bi_2O_3 NRs in the range of 400–4000 cm^{-1}. Figure 5 depicts the raw FTIR-transmittance spectrum of α-Bi_2O_3 NRs at RT, including a sharp absorption peak at 1388 cm^{-1} and two absorption peaks at 844 cm^{-1} and 554 cm^{-1}, which looks very similar to the corresponding FTIR-transmittance spectrum of α-Bi_2O_3 nanorods, as reported in the same frequency range in [16]. The sharp absorption peak at 1388 cm^{-1} may be due to the C–O vibration modes of ethanol molecules that may absorbed during α-Bi_2O_3 NRs synthesize process or related to stretching modes of NO_3^- ion [37]. The bands located at 844 cm^{-1} and 554 cm^{-1} are assigned to the stretching vibration modes of Bi–O bonds of BiO_6 octahedron. Above that range, the FTIR-transmittance looks flat without any significant structure.

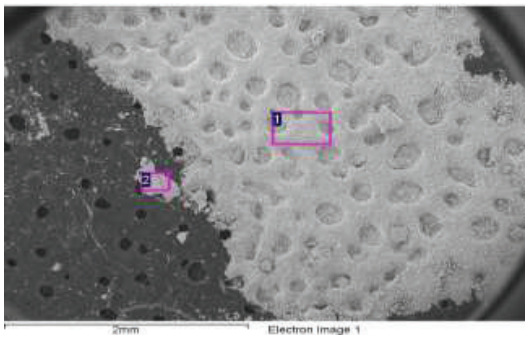

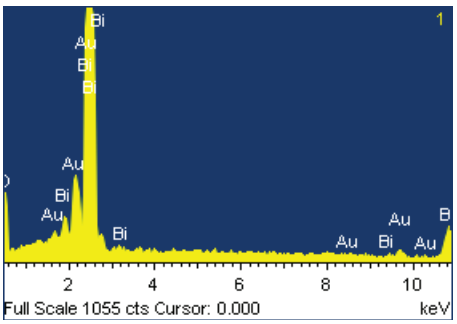

Processing option : All elements analysed (Normalised)

Spectrum	In stats.	C	O	Bi
1	Yes	49.52	40.20	10.28
2	Yes	56.36	35.84	7.76
Max.		56.36	40.20	10.28
Min.		49.52	35.84	7.76

All results in atomic %

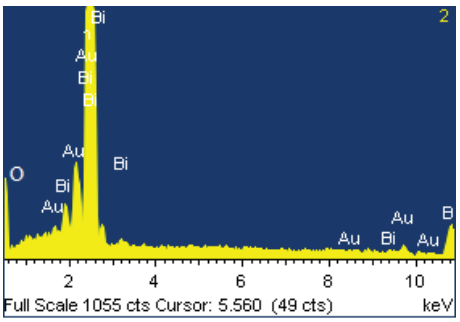

Figure 2. Energy dispersive x-ray spectroscopy (EDXS) spectra with EDXS data of α-Bi_2O_3 NRs. Note: the presence of Au peaks shown in the spectrum and carbon ratio in the table came from the gold catalyst and the carbon-coated cupper grid on which Bi_2O_3 sample was supported respectively.

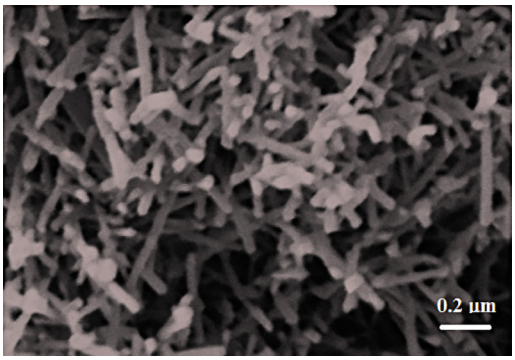

Figure 3. Field emission scanning electron microscopy (FE-SEM) image of α-Bi_2O_3 NRs.

This evidence is in good agreement with the reported in literature [16, 19] and makes our results consistent with those of XRD shown in figure 1.

3.4. UV–Vis diffuse reflectance spectroscopy (UV–Vis DRS) analysis

Among the optical methods, Measurement of diffuse reflectance of a powder samples with UV–Vis diffuse reflectance spectroscopy (UV–Vis DRS) is one of the most important techniques in the determination of the optical properties of semiconductor materials [38]. Indeed, UV–Vis DRS is an effective spectroscopic tool to estimate the optical band gap of powder samples unambiguously. The powder sample should be thick enough that all incidents light is absorbed or scattered before reaching the back surface of the sample (i.e. typically a thickness of 2–4 mm is required). Kubelka–Munk theory provides the theoretical descriptions of diffuse reflectance process for powdered samples. The Kubelka–Munk equation is expressed as follows [39]:

$$F(R) = \frac{(1-R)^2}{2R} = \frac{k}{s} \tag{4}$$

where: $F(R)$ is proportional to the extinction coefficient, R is the absolute reflectance of the sampled layer, s is the scattering coefficient and k is the absorption coefficient. The transformed Kubelka–Munk function can be obtained by multiplying the $F(R)$ function by energy ($h\nu$) according to the following expression:

$$[F(R) * h\nu]^f \tag{5}$$

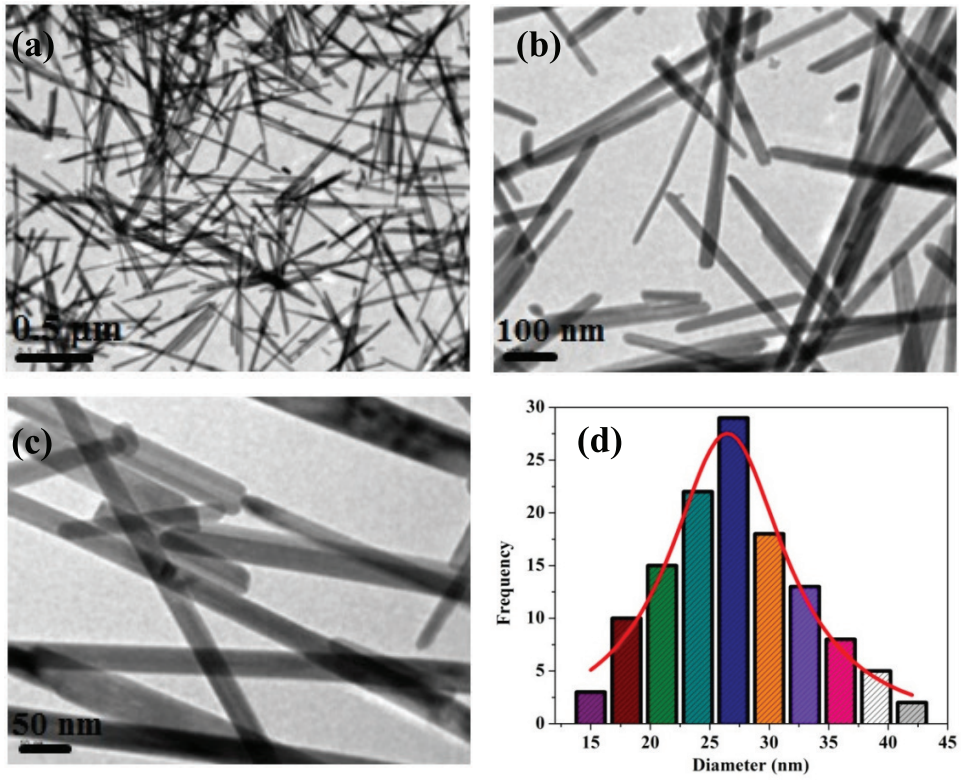

Figure 4. TEM micrographs of α-Bi_2O_3 NRs at different magnifications (a)–(c) with diameter distribution histogram (d).

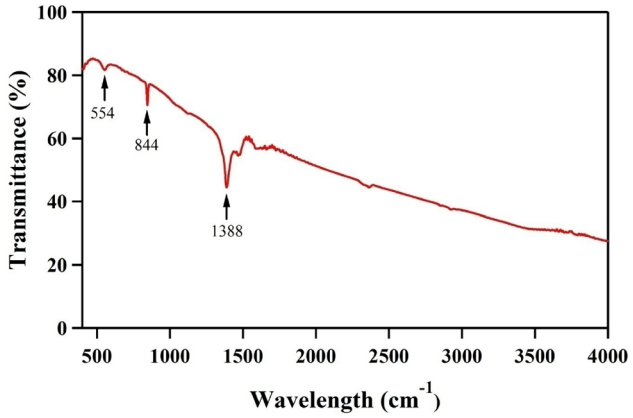

Figure 5. FTIR-transmittance spectrum of as-synthesized α-Bi_2O_3 NRs.

Where $f = 2$ or 1/2 for direct allowed transition or indirect allowed transition respectively. By plotting this expression as a function of the energy ($h\nu$) in eV, one can obtain the direct and indirect optical band gap of α-Bi_2O_3 NRs by extrapolating the straight part of the graph on energy axis. Figure 6(a) depicts the corresponding diffuse reflectance spectrum of the as-synthesized α-Bi_2O_3 NRs. From the plot of $[F(R)h\nu]^f$ versus ($h\nu$) where $f = 2$ or 1/2 (figures 6(b) and (c)), the optical band gap of α-Bi_2O_3 NRs is estimated as 3.63 eV and 3.55 eV for a direct allowed transition and an indirect allowed transition respectively; Many researchers have been reported that, the difference between the direct and indirect transition for α-Bi_2O_3 of about 0.1 eV [40, 41]. It is worth to indicate that, the estimated optical band gaps were significantly higher than the reported bulk values (2.8–2.93 eV) [40], which might be attributed to the reduction in α-Bi_2O_3 NRs diameters (15–42 nm); Therefore, according to these gap values (3.55 eV and 3.63 eV); we need to use UV irradiation source, in order to examine the photocatalytic activity of α-Bi_2O_3 NRs.

3.5. Photocatalytic activity of α-Bi_2O_3 NRs

Photocatalytic reaction process occurs when semiconducting nanoparticles are subjected to light irradiation causing accelerated chemical reactions. Such processes give rise to free radical species [O^- and $OH^{\blacksquare}$] which can react with organic pollutants leading to their mineralization and then their degradation. Figure 7 shows the schematic illustration of photocatalytic reaction taking place on the surface of α-Bi_2O_3 NRs photocatalyst under

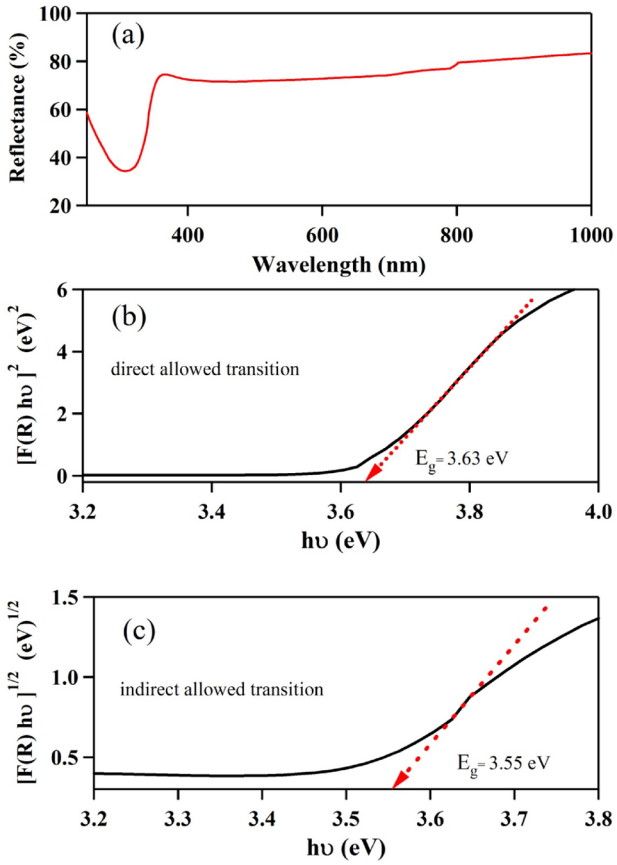

Figure 6. (a) The diffuse reflectance spectrum of the as-synthesized α-Bi_2O_3 NRs. (b) and (c) The calculation of the optical energy gap (E_g) of α-Bi_2O_3 NRs using the transformed Kubelka–Munk function versus energy ($h\nu$) plot (b) direct allowed transition (c) indirect allowed transition.

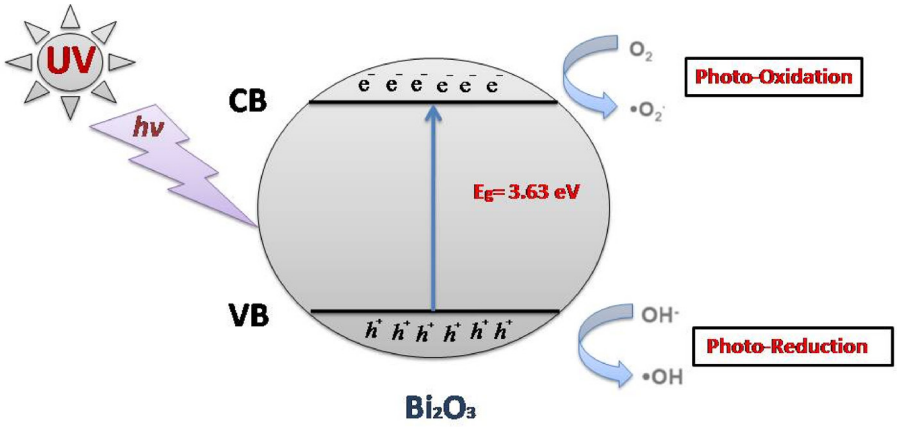

Figure 7. Schematic of the photocatalytic reaction mechanism for MB dye in the presence of α-Bi_2O_3 NRs photocatalyst.

UV light illumination. Since, the optical band gap of synthesized α-Bi_2O_3 NRs is between 3.55 eV and 3.63 eV, it can easily be stimulated by UV radiations. As it can be observed from figure 7, a photocatalyst such as α-Bi_2O_3 NRs in contact with organic pollutants under UV light illumination absorbs such radiation, which corresponds to its optical band gap and then the electrons in the valence band (VB) are excited into the conduction band (CB), leaving behind an equal number of holes in the VB of the α-Bi_2O_3 photocatalyst (equation (6)).

$$\alpha - Bi_2O_3 + h\nu \rightarrow \alpha - Bi_2O_3\,[e^- + h^+] \tag{6}$$

The activation of α-Bi_2O_3 NRs by UV light produces electron–hole pairs which are powerful oxidizing and reducing agents, respectively. Oxygen is commonly used as electron acceptor. It may react with photo-generated electron at the surface of α-Bi_2O_3 NRs through the following equations.

$$O_2 + e^- \rightarrow O_2^{\blacksquare -} \tag{7}$$

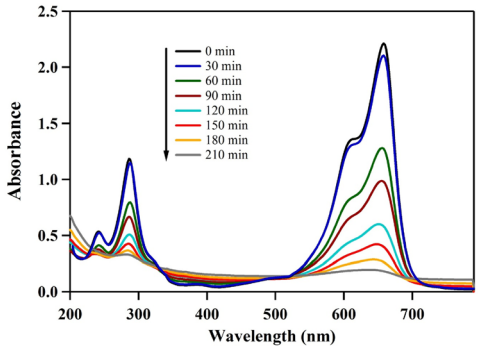

Figure 8. The UV–Vis absorbance versus wavelength as a function of UV illumination time of methylene blue (MB) in the presence of α-Bi_2O_3 NRs photocatalyst.

$$O_2^{\blacksquare -} + H^+ \rightarrow HO_2^{\blacksquare} \tag{8}$$

$$HO_2^{\blacksquare} + HO_2^{\blacksquare} \rightarrow H_2O_2 + O_2 \tag{9}$$

$$H_2O_2 + O_2^{\blacksquare -} \rightarrow {}^{\blacksquare}O\,H + OH^- + O_2 \tag{10}$$

The photo-induced holes, having affinity for electrons, are very strong oxidizing agents. After migrating to the surface of the α-Bi_2O_3 NRs, they oxidize the adsorbed water molecule or hydroxide ion to form hydroxyl radicals according to the following equations:

$$h^+ + H_2O \rightarrow {}^{\blacksquare}O\,H + H^+ \tag{11}$$

$$h^+ + {}^-O\,H \rightarrow {}^{\blacksquare}OH \tag{12}$$

Therefore, the overall photocatalytic degradation mechanism can be summarized through the following reaction.

$$MB\ \text{dye} + O_2^{\blacksquare -} \text{ or } {}^{\blacksquare}OH \rightarrow CO_2\uparrow + H_2O + \text{decomposed products} \tag{13}$$

Then all these highly oxidizing species ($^-$OH, $^{\bullet}$OH, H_2O_2, etc) are capable of oxidizing organic molecules, such as MB into simpler molecules such as CO_2, H_2O, etc (equation (13)).

The photocatalytic activity of the as-synthesized α-Bi_2O_3 NRs was examined using MB as a pollutant model under UV light illumination. Figure 8 shows the photocatalytic degradation of MB in the presence of α-Bi_2O_3 NRs as photocatalyst under UV illumination at different irradiation time from 0 to 210 min. In our obtained results, the UV–Vis absorbance spectra for the degradation of MB in the presence of α-Bi_2O_3 NRs photocatalyst revealed that the intensity of the two main peaks of MB at $\lambda = 286$ nm and $\lambda = 658$ nm were diminished gradually with the increase of UV illumination time. Under UV irradiation the MB was degraded completely by using α-Bi_2O_3 NRs photocatalyst after 210 min, which indicates that α-Bi_2O_3 NRs shows UV-photocatalytic activity in the degradation of MB. The characteristic absorption of MB at 658 nm was selected to monitor the photocatalytic response process. By the relation between the concentration (C) and the absorbance (A) of MB at time t according to the Beer–Lambert law, one can estimate the degradation efficiency percentage (η) of MB by the following expression [42]:

$$\eta = \frac{C_0 - C}{C_0} \times 100\% = \frac{A_0 - A}{A_0} \times 100\% \tag{14}$$

where C_0 and A_0 are the initial concentration and initial absorbance of MB dye at time t_0 respectively. It is worth to indicate that the change in the absorbance peaks of MB without Bi_2O_3 photocatalyst under UV irradiation is found to be negligible. Figure 9 depicts the percentage degradation efficiency of MB as a function of UV- illumination time in the presence of α-Bi_2O_3 NRs photocatalyst. The concentration of MB has decreased by half after 90 min of irradiation time, whereas MB was completely photodegraded after 210 min under UV irradiation using α-Bi_2O_3 NRs as photocatalyst. The photocatalytic decolourization of most organic pollutants has been described by using modified Langmuire–Hinshelwood (L–H) kinetic model [43, 44], which can be expressed with the following equation:

$$\ln\left(\frac{C_0}{C}\right) = k_{obs}t \tag{15}$$

By assuming that $C = C_0$ at $t = 0$ with low initial MB dye concentration, where t is the particular irradiation time and k_{obs} is the observed pseudo-first-order rate constant, which is usually chosen as the main kinetic parameter

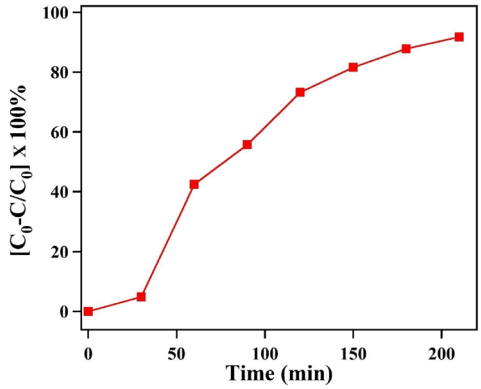

Figure 9. Percentage degradation efficiency of methylene blue (MB) as a function of UV-illumination time (t) in the presence of α-Bi_2O_3 NRs photocatalyst.

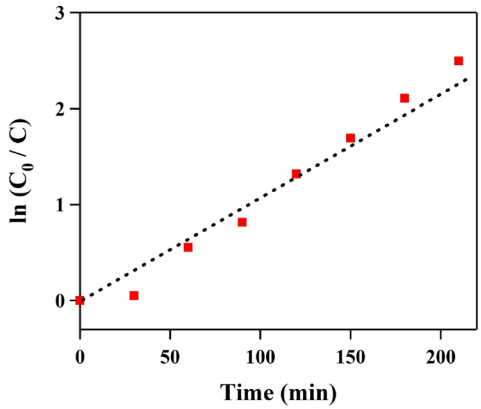

Figure 10. Linear plot of $\ln(C_0/C)$ for the photodegradation of methylene blue (MB) as a function of UV-irradiation time (t) in the presence of α-Bi_2O_3 NRs photocatalyst.

for the comparison of different photocatalysts. According to equation (15) the plot of $\ln(C_0/C)$ versus t should be linear and the value of k_{obs} can be estimated directly via its slope (figure 10). The slope of the plot which represents the photocatalyst reaction rate is 10×10^{-3} min^{-1}. The photocatalytic activity of α-Bi_2O_3 NRs, prepared in current study, showed better degradation efficiency of MB under UV irradiation compared to what was found by Sangchay [45], Bubacz *et al* [46], Rajesh *et al* [47], and Chakrabarti [48]. Sangchay reported that for TiO_2 powder, prepared by sol-gel method, the degradation percentage of MB under UV irradiation for 6 h is 82%, while the commercial P25 was only 47%. Bubaczand and Rajesh, showed that MB was completely photodegraded after 6 h under UV irradiation using TiO_2 as a photocatalyst. Lastly, Sampa reported that ZnO showed relatively low degradation efficiency under UV irradiation (~58% after 120 min). In short, we report that the photocatalytic degradation efficiency of α-Bi_2O_3 NR photocatalyst is high compared to published studies on photocatalytic degradation of MB by commercial semiconductor oxides.

4. Conclusions

In conclusion, high quality monoclinic bismuth oxide nanorods (α-Bi_2O_3 NRs), with diameters between (15–42 nm) and lengths of several micrometers have been successfully prepared by a simple hydrothermal route. The product was characterized in detail by different techniques, such as XRD, EDXS, TEM, FTIR and UV–Vis DRS. According to XRD analysis it was found that, the as-synthesized Bi_2O_3 powder sample exhibited high purity with monoclinic structure and good crystallinity. The EDAX and TEM analysis revealed that, the as-synthesized α-Bi_2O_3 has high purity and stoichiometric composition with nanorod morphology. FTIR measurement confirmed the stretching vibration modes of Bi–O bonds of Bi_2O_3 located at 554 cm^{-1} and 844 cm^{-1}. UV–Vis DRS analysis using Kubelka–Munk theory showed that, the optical band gap values of α-Bi_2O_3 NRs are 3.63 eV and 3.55 eV for a direct allowed transition and an indirect allowed transition respectively. The photocatalytic properties of α-Bi_2O_3 NRs as an effective photocatalyst for the degradation of MB under UV irradiation were found to be attractive. The kinetics of photocatalytic degradation of MB has been investigated

according to modified Langmuire–Hinshelwood (L–H) kinetic model. The results of photodegradation of α-Bi_2O_3 NRs indicate that MB was completely photodegraded after 210 min under UV irradiation with a reaction rate of 10×10^{-3} min^{-1}.

References

[1] Zhu G and Xu Z 2011 *J. Am. Chem. Soc.* **133** 148–57
[2] Kumari L, Lin J-H and Ma Y-R 2007 *J. Phys.: Condens. Matter* **19** 406204
[3] Xie X, Li Y, Liu Z-Q, Haruta M and Shen W 2009 *Nature* **458** 746–9
[4] Zhuiykov S 2014 *Nanostructured Semiconductor Oxides for the Next Generation of Electronics and Functional Devices* (Cambridge: Woodhead Publishing)
[5] Sabirin Zoolfakar A, Rani R A, Morfa A J, O'Mullaned Anthony P and Kalantar-zadeh K 2014 *J. Mater. Chem.* C **2** 5247–70
[6] Pan Z W, Dai Z R and Wang Z L 2001 *Science* **291** 1947–9
[7] Huang J and Wan Q 2009 *Sensors* **9** 9903–24
[8] Li Z, Sun Q, Yao X D, Zhu Z H and (Max) Lu Gao Q 2012 *J. Mater. Chem.* **22** 22821–31
[9] Eda S, Fujishima M and Tada H 2012 *Appl. Catal.* B **125** 288–93
[10] Liu Y, Wang Z, Huang B, Zhang X, Qin X and Dai Y 2010 *J. Colloid Interface Sci.* **348** 211–5
[11] Chen X Y, Zhang Z J and Lee S W 2008 *J. Solid State Chem.* **181** 166–74
[12] Cabot A, Marsal A, Arbiol J and Morante J R 2004 *Sensors Actuators* B **99** 74–89
[13] Fruth A V, Ianculescu A, Berger D, Preda S, Voicu E, Tenea G and Popa M 2006 *J. Eur. Ceram. Soc.* **26** 3011–6
[14] Zhang G, Yang J, Zhang S, Xiong Q, Huang B, Wang J and Gong W 2009 *J. Hazard. Mater.* **172** 986–92
[15] Ren J, Wang W Z, Shang M, Sun S M and Gao E P 2011 *ACS Appl. Mater. Int.* **3** 2529–33
[16] Sood S, Umar A, Mehta S K and Kansal S K 2015 *Ceram. Int.* **41** 3355–64
[17] Yilmaz S, Turkoglu O, Ari M and Belenli I 2011 *Ceramica* **57** 185–92
[18] Hu J, Xu G, Wang J, Lv J, Zhang X, Xie T, Zheng Z and Wu Y 2015 *Dalton Trans.* **44** 5386–95
[19] Raza W, Khan A, Alam U, Muneer M and Bahnemann D 2016 *J. Mol. Struct.* **1107** 39–46
[20] Salima Y, Al-Dourib M S, Al Waznyc E T and Fakhrib M A 2014 *Sol. Energy* **107** 523–9
[21] Proffit G-R, Bai D D, Fong T T, Fister S O, Hruszkewycz M J, Highland P M, Baldo P H, Fuoss T O, Mason J A and Eastman D L 2010 *Appl. Phys. Lett.* **96** 021905
[22] Wang L, Cui Z-L and Zhang Z-K 2007 *Surf. Coat. Technol.* **201** 5330–2
[23] Fan S S, Pan X M, Teng C, Ye G H, Li L D and Zhang H T 2006 *Thin Solid Films* **513** 142–7
[24] Ho C-H, Chan C-H, Huang Y-S, Tien L-C and Chao L-C 2013 *Opt. Express* **21** 11965–72
[25] Iyyapushpam S, Nishanthi S T and Pathinettam Padiyan D 2012 *Mater. Lett.* **86** 25–7
[26] Shen X-P, Wu S-K, Zhao H and Liu Q 2007 *Physica* E **39** 133–6
[27] Kim H W, Myung J H and Shim S H 2006 *Solid State Commun.* **137** 196–8
[28] Wu C, Shen L, Huang Q and Zhang Y-C 2011 *Mater. Lett.* **65** 1134–6
[29] Byrappa K and Adschiri T 2007 *Prog. Cryst. Growth Charact. Mater.* **53** 117–66
[30] El-Remaily M A A A and Abu-Dief A M 2015 *Tetrahedron* **71** 2579–84
[31] Abu-Dief A M, Abdelbakyb M S M, Martı´nez-Blanco D, Amghouz Z and Garcı´a-Granda S 2016 *Mater. Chem. Phys.* **174** 164–71
[32] Kropid Lowska A, Chojna Cki J, Fahmi A and Becker B 2008 *Dalton Trans.* **47** 6825–31
[33] Bilgin V, Kose S, Atay F and Akyuz I 2005 *Mater. Chem. Phys.* **94** 103–8
[34] Khan Z R, Zulfequar M and Khan M S 2010 *Mater. Sci. Eng.* B **174** 145–9
[35] Abdel-Rahman L H, Abu-Dief M A, El-Khatib R M and Abdel-Fatah S M 2016 *J. Photochem. Photobiol.* B **162** 298–308
[36] Abdel-Rahman L H, Abu-Dief A M, Adam M S S and Hamdan S K 2016 *Catal. Lett.* **146** 1373–96
[37] Abdel-Rahman L H, Abu-Dief A M, Newair E F and Hamdan S K 2016 *J. Photochem. Photobiol.* B **160** 18–3
[38] Nowak M, Kauch B and Szperlich P 2009 *Rev. Sci. Instrum.* **80** 046107
[39] Lopez R and Gomez R 2012 *J Sol-Gel Sci. Technol.* **61** 1–7
[40] Eberl J and Kisch H 2008 *Photochem. Photobiol. Sci.* **7** 1400–6
[41] Carlsson J M, Hellsing B, Domingos H S and Bristowe P D 2002 *Phys. Rev.* B **65** 205122
[42] Abdollahi Y, Abdullah A H, Zainal Z and Yusof N A 2011 *Int. J. Mol. Sci.* **13** 302–15
[43] Houas A, Lachheb H, Ksibi M, Elaloui E and Guillard C 2001 *Jean-Marie Herrmann Appl. Catal.* B **31** 145–57
[44] Wang N, Tan F, Wan L, Wu M and Zhang X 2014 *Biomicrofluidics* **8** 054122
[45] Sangchay W 2013 *Adv. Mater. Res.* **626** 334–8
[46] Bubacz K, Choina J, Dolat D and Morawski A W 2010 *Polish J. Environ. Stud.* **19** 685–91
[47] Tayade R J, Natarajan T S and Bajaj H C 2009 *Ind. Eng. Chem. Res.* **48** 10262–7
[48] Chakrabarti S and Dutta B K 2004 *J. Hazard. Mater.* B **112** 269–78